ACS OMEGA

Article

Cite This: ACS Omega 2019, 4, 3660−3672

http://pubs.acs.org/journal/acsodf

Electrospun Conducting and Biocompatible Uniaxial and Core−Shell Fibers Having Poly(lactic acid), Poly(ethylene glycol), and Polyaniline for Cardiac Tissue Engineering

Paula T. Bertuoli,[†,‡,§] Jesús Ordoño,[∥,⊥] Elaine Armelin,[‡,§] Soledad Pérez-Amodio,[∥,⊥,#] Alessandra F. Baldissera,[¶] Carlos. A. Ferreira,[¶] Jordi Puiggalí,[‡,§] Elisabeth Engel,[*,∥,⊥,#] Luis J. del Valle,[*,‡,§] and Carlos Alemán[*,‡,§]

[†]Programa de Pós-Graduação em Engenharia de Minas, Metalúrgica e Materiais (PPGE3M), and [¶]Departamento de Materiais (DEMAT), Universidade Federal do Rio Grande do Sul (UFRGS), Avenida Bento Gonçalves, 9500, 91501-970 Porto Alegre, Rio Grande do Sul, Brazil

[‡]Departament d'Enginyeria Química, EEBE, Universitat Politècnica de Catalunya, C/Eduard Maristany, 10-14, Ed. I2, 08019 Barcelona, Spain

[§]Barcelona Research Center for Multiscale Science and Engineering, Universitat Politècnica de Catalunya, Eduard Maristany, 10-14, 08019 Barcelona, Spain

[∥]Institute for Bioengineering of Catalonia (IBEC), The Barcelona Institute of Science and Technology, Baldiri Reixac 10-12, 08028 Barcelona, Spain

[⊥]CIBER en Bioingeniería, Biomateriales y Nanomedicina, CIBER-BBN, Zaragoza 50018, Spain

[#]Materials Science and Metallurgical Engineering, EEBE, Universitat Politècnica de Catalunya (UPC), C/Eduard Maristany, 10-14, Ed. I2, 08019 Barcelona, Spain

S *Supporting Information*

ABSTRACT: Electroactive and biocompatible fibrous scaffolds have been prepared and characterized using polyaniline (PAni) doped with dodecylbenzenesulfonic acid (DBSA) combined with poly(lactic acid) (PLA) and PLA/poly(ethylene glycol) (PEG) mixtures. The composition of simple and core−shell fibers, which have been obtained by both uniaxial and coaxial electrospinning, respectively, has been corroborated by Fourier-transform infrared and micro-Raman spectroscopies. Morphological studies suggest that the incorporation of PEG enhances the packing of PLA and PAni chains, allowing the regulation of the thickness of the fibers. PAni and PEG affect the thermal and electrical properties of the fibers, both decreasing the glass transition temperature and increasing the electrical conductivity. Interestingly, the incorporation of PEG improves the PAni-containing paths associated with the conduction properties. Although dose response curves evidence the high cytotoxicity of PAni/DBSA, cell adhesion and cell proliferation studies on PLA/PAni fibers show a reduction of such harmful effects as the conducting polymer is mainly retained inside the fibers through favorable PAni···PLA interactions. The incorporation of PEG into uniaxial fibers resulted in an increment of the cell mortality, which has been attributed to its rapid dissolution into the culture medium and the consequent enhancement of PAni release. In opposition, the delivery of PAni decreases and, therefore, the biocompatibility of the fibers increases when a shell coating the PAni-containing system is incorporated through coaxial electrospinning. Finally, morphological and functional studies using cardiac cells indicated that these fibrous scaffolds are suitable for cardiac tissue engineering applications.

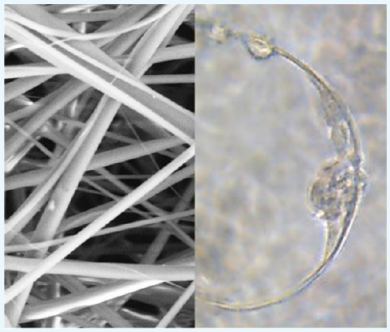

INTRODUCTION

Lots of conductive biomaterials have been tested for their application as smart scaffolds for tissue repair and regeneration.[1−9] In addition to graphene,[1,2] gold nanoparticles,[3] carbon nanotubes,[4] and so forth, nondegradable conducting polymers (CPs) have been successfully blended and composited with biodegradable polymers for such biomedical applications.[5−11] One of the most important questions for the application in tissue engineering of CPs, which are highly compatible with many biological molecules and living systems, is their inherent inability to degrade. This limits the in vivo application of these materials and the scaffolds may require surgical removal. Therefore, combining CPs with biodegradable polymers to obtain materials with electroactive and biodegradable properties at the same time has received growing interest.

Received: December 5, 2018
Accepted: January 30, 2019
Published: February 19, 2019

DOI: 10.1021/acsomega.8b03411
ACS Omega 2019, 4, 3660−3672

Among CPs, polypyrrole and polythiophene (PTh) derivatives have been the most employed for tissue regeneration applications because of their biocompatibility.[5−15] In contrast, biomedical applications of polyaniline (PAni) are controversial because of the uncertainty in its cytotoxicity, which in the best case is considered to present time- and/or dose-dependent hazardous potential.[16−20] However, PAni has a number of advantages, including high electrical conductivity, excellent electronic and optical properties, good redox and ion-exchange activity, environmental stability, ease of preparation from common chemicals, and low cost.[21,22]

On the other hand, poly(lactic acid) (PLA) is a 100% biodegradable biopolymer that is manufactured from lactic acid, a renewable resource derived from the starch of either corn or sugar beets that is fermented to form glucose and, consequently, converted to lactic acid. Accordingly, PLA is an important compound within the green chemistry context, as it reduces significantly the carbon foot print when compared to other oil-based traditional plastics. In addition to its usage in different commercial and technological applications (e.g., automotive parts, clothing and carpet fibers, and food packaging), PLA and its copolymers are widely employed in the biomedical field because of the good mechanical integrity, biodegradability, and biocompatibility. Thus, these materials have been employed for the fabrication of drug-loading and -release devices, surgical sutures, and scaffolds for tissue and nerve regeneration.[23−28]

In spite of the uncertainty in their cytotoxicity, aniline oligomers[29−39] and PAni[39−45] have emerged as electroactive moieties in tissue engineering. In some cases, these electroactive compounds have been combined with PLA. For example, biodegradable conductive polymers were synthesized by conjugating small aniline oligomers with PLA to produce block copolymers[31,32] and hyperbranched functionalized polyesters[33,34] More recently, Liu et al.[35] prepared an electroactive diblock copolymer by conjugating poly(ethylene glycol) (PEG) methyl ether and aniline tetramer (AT), which was subsequently blended with PLA to decrease the cytotoxicity of AT. On the other hand, Cui et al.[36] prepared electroactive biodegradable hydrogels from carboxyl-capped-AT/PLA/PEG/PLA/carboxyl-capped-AT copolymers. That work was inspired by the approach previously developed by Albertsson and co-workers,[37] which synthesized hydrogels with similar properties using acrylated PLA/PEG/PLA with AT. Also, the same group transformed the surface of PLA into conductive and hydrophilic by grafting AT units.[38] Wu et al.[39] reported novel conductive biodegradable polyurethane based on the poly(glycerol sebacate)-*co*-aniline pentamer to enhance Schwann cells' myelin gene expressions and neurotrophin secretion for peripheral nerve regeneration.

McKeon et al.[41] electrospun PLA and PAni together to create biodegradable, biocompatible, and electrically conductive scaffolds. Although nanofibers were successfully attained with various PLA/PAni ratios, only the 75:25 scaffold conducted a significant current. Nevertheless, the high amount of PAni released upon degradation of PLA prevented this blend from being used as the primary component in biomedical devices.[41] This problem was mitigated by preparing PLA/PAni electrospun nanofibrous sheets with a lower content of PAni (1.5 to 3 wt %) doped with camphorsulfonic acid.[42] The resulting scaffolds exhibited good cell viability and a promoting effect on differentiation of H9c2 cardiomyoblasts in terms of maturation index and fusion index. Zhao et al.[43] developed a new series of in situ-forming antibacterial-conductive degradable hydrogels using quaternized chitosan (QCS)-grafted PAni with oxidized dextran as crosslinker. The electroactive hydrogels could significantly enhance the proliferation of C2C12 myoblasts compared to the QCS hydrogel. Al-Jallad et al.[44] developed an oxidative solution polymerization of PAni onto electrospun nonwoven fiber mats of PLA. However, in this case no biomedical application was proposed because of the high content of PAni. In a very recent work, PAni nanoparticles polymerized from aniline in a PLA solution were used to produce an electrically conductive nanofibrous composite by thermal-induced phase separation.[45] These scaffolds promoted osteogenic differentiation of bone marrow-derived mesenchymal stem cells for bone engineering.

Among the potential applications in tissue engineering of CPs, cardiac tissue regeneration is of special interest because of their intrinsic electrical behavior. The generation of electrical impulses by pacemaker cells together with a complex network of interconnected cardiomyocytes results in a coordinated contraction and maintenance of the heart rhythm.[46−48] Cardiovascular diseases are the world's leading cause of mortality,[49] and typical strategies for cardiac tissue engineering rely on the generation of a functional cardiac graft for implantation and the use of different biomaterials for engraftment of stem cells. However, one of the main issues associated with the development of such cardiac constructs for regenerative therapies is the poor electrical integration of the construct with the host tissue. This integration is critical to prevent secondary complications related to graft and host asynchrony, frequently leading to arrhythmias, which can be fatal if untreated.[50−52] Additionally, electrical stimulation of cardiac cells and specially stem cell-derived cardiomyocytes has been proven to stimulate maturation and improve cardiac functions.[53−57] Similarly, the development of cardiac tissues for drug screening also requires electrical interconnectivity to truly reproduce tissue behavior.[58] Thus, the use of conductive biomaterials as scaffolds for cardiac cells is a very promising tool and has already been demonstrated to be valuable for cardiac cell function.[59,60] In a recent study, a sophisticated PAni-based conductive scaffold for cardiac tissue engineering was reported by Guo and co-workers.[61] This consisted in a hybrid scaffold based on aligned poly(caprolactone), silk fibroin, and PAni nanofiber yarn network layers within a hydrogel shell for mimicking the native tissue structure, which demonstrated its great potential for engineering 3D cardiac constructs.

In this work, we propose a new strategy using soluble PAni doped with dodecylbenzenesulfonic acid (DBSA), prepared by one-step emulsion polymerization, to electrospin fibrous scaffolds with PLA or PLA/PEG mixtures. The advantage of concomitantly employing PLA and PEG is the ease in the processing ability of the former, the high biocompatibility of the latter, and the plasticizer effect of PEG, which is expected to regulate the structure and properties of the PLA/PAni fibers.[62−65] Uniaxial and coaxial electrospinning have been used to obtain simple and core−shell fibers, respectively. More specifically, uniaxial fibers have been electrospun using PLA/PAni and PLA/PEG/PAni mixtures with different ratios, whereas polymer solutions based on PLA/PAni (core) and PLA or PLA/PEG (shell) mixtures have been used for coaxial electrospinning. The incorporation of PAni and PEG in the structural, spectroscopic, thermal, and electrical properties of PLA electrospun fibers has been examined. After this, the cytotoxicity of PAni doped with DBSA, hereafter PAni/DBSA, and the biocompatibility of the different uniaxial and core−shell

DOI: 10.1021/acsomega.8b03411
ACS Omega 2019, 4, 3660−3672

Table 1. Nomenclature, Preparation Conditions, and Composition of All Fibers Prepared in This Work

fibers	preparation and composition
PLA	control uniaxial fibers electrospun from a 16.6% w/v PLA solution in chloroform/acetone (2:1 v/v)
PLA/PAni-*n* %, with *n* = 2.5, 5, 7.5, or 10	uniaxial fibers electrospun from PLA/PAni mixtures with *n* % w/w PAni (relative to PLA) dissolved in chloroform at a polymer concentration of 16.6% w/v. The general acronym (i.e., independently of the PAni concentration) for these fibers is PLA/PAni
PLA/PEG-*m*/PAni with *m* = 0.1 or 0.3	uniaxial fibers electrospun from a $(1 - m)/m$ PLA/PEG chloroform solution at a polymer concentration of 16.6% w/v with 5% w/w of PAni relative to PLA/PEG. The general acronym (i.e., independently of the PEG content) for these fibers is PLA/PEG/PAni
PLA-*m*/PAni with *m* = 0.1 or 0.3	uniaxial fibers obtained by etching the PEG of PLA/PEG-*m*/PAni fibers with water. No general acronym has been used for these fibers
PLA//PLA/PAni	coaxial fibers in which the shell was electrospun from an 8.3% w/v PLA solution in chloroform and acetone, whereas the core was electrospun using a PLA/PAni mixture with 5% w/w PAni (relative to PLA) dissolved in chloroform at a polymer concentration of 8.3% w/v
PLA/PEG-*m*//PLA/PAni with *m* = 0.1 or 0.3	coaxial fibers in which the shell was electrospun from a $(1 - m)/m$ PLA/PEG chloroform solution at a polymer concentration of 8.3% w/v, whereas the core was electrospun using a PLA/PAni mixture with 5% w/w of PAni (relative to PLA) dissolved in chloroform at a polymer concentration of 8.3% w/v. The general acronym (i.e., independently of the PEG content) for these fibers is PLA/PEG//PLA/PAni
PLA-*m*//PLA/PAni	coaxial fibers obtained by etching the PEG of PLA/PEG-*m*//PLA/PAni fibers with water. No general acronym has been used for these fibers

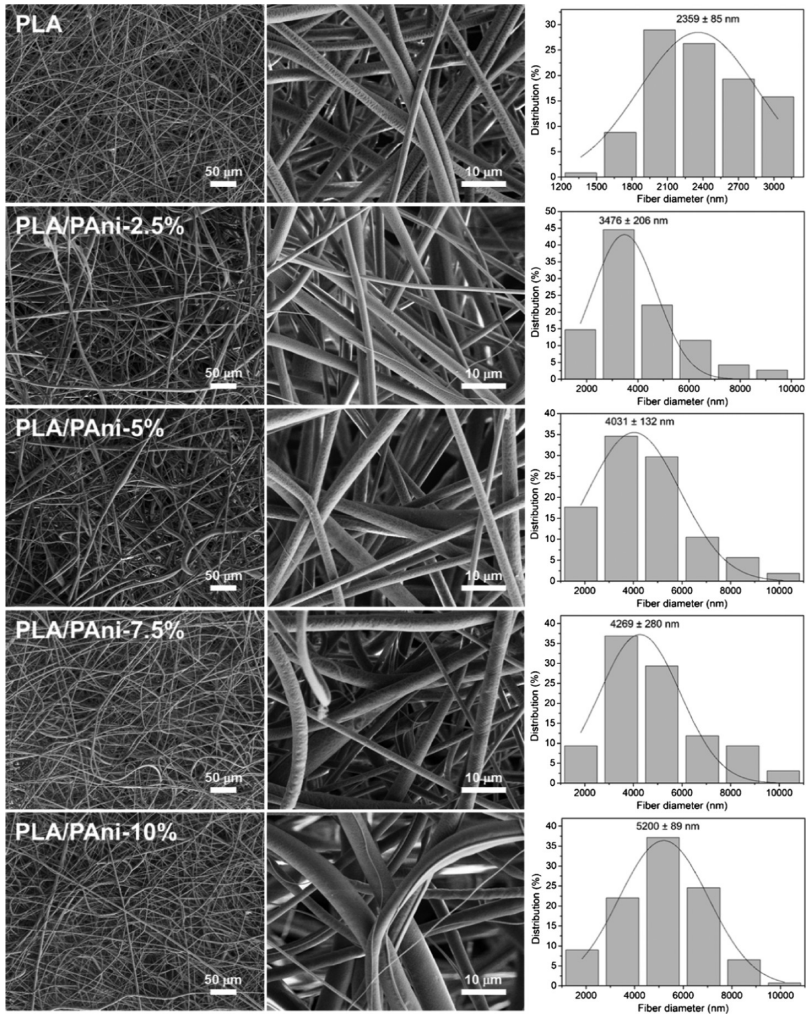

Figure 1. SEM micrographs taken at low (left) and high (center) magnification for electrospun fibers of PLA and PLA/PAni-2.5, -5, -7.5, and -10% samples. The diameter distribution of the electrospun microfibers is displayed at the right.

PAni-containing fibers have been examined. Finally, the suitability of the new scaffolds for cardiac tissue engineering applications was evaluated using cardiac primary cells isolated from neonatal mice hearts.

RESULTS AND DISCUSSION

Details about the labels used to denote the different scaffolds prepared in this work are provided in the Methods section. However, in order to facilitate the understanding of the results, Table 1 summarizes the nomenclature and composition of all fibers prepared in this work.

DOI: 10.1021/acsomega.8b03411
ACS Omega 2019, 4, 3660−3672

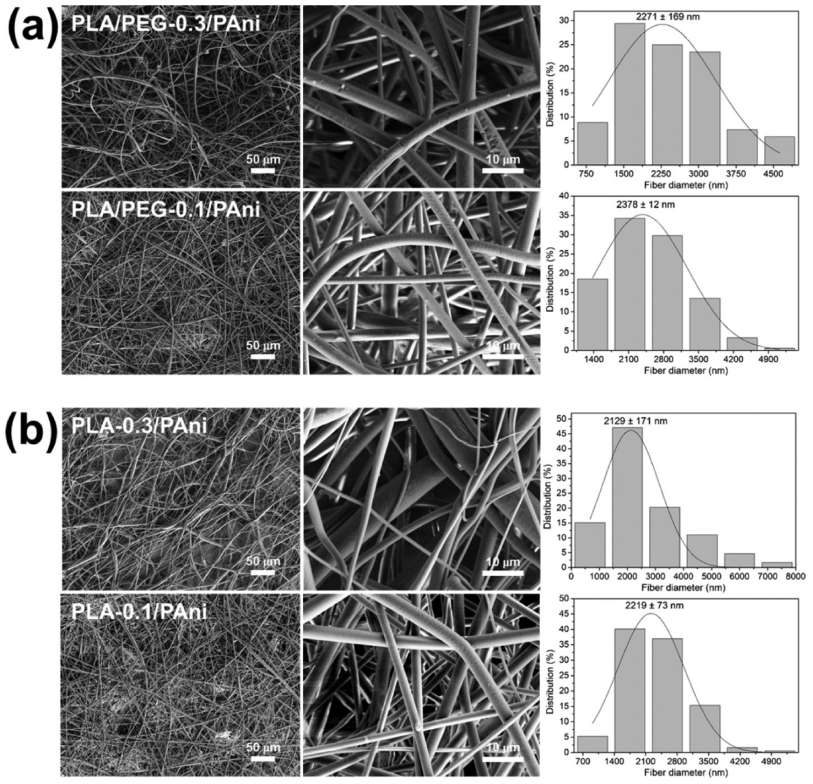

Figure 2. SEM micrographs taken at low (left) and high (center) magnification for electrospun fibers of (a) PLA/PEG-0.3/PAni and PLA/PEG-0.1/PAni samples and (b) PLA-0.3/PAni and PLA-0.1/PAni samples. The diameter distribution of the electrospun microfibers is displayed at the right.

Morphology. Representative scanning electron microscopy (SEM) micrographs of PLA, PLA/PAni-2.5, -5, -7.5, and -10% fibers (Table 1) captured at different magnifications are displayed in Figure 1. In all cases, long and abundant microfibers with cylindrical morphology, which were randomly distributed in porous fibrous mats, were attained. High-magnification micrographs indicate that the surface texture of the fibers did not undergo major changes with the composition, even though the slightly rough appearance of the PLA surface changes to a smoother aspect in PLA/PAni. Figure 1 includes the monomodal diameter distributions (around 200 measures were considered for each system) observed for the samples prepared under the optimized conditions described in the Methods section. The diameter distribution is wider for PLA/PAni fibers than for PLA fibers. In general, diameters so different as 2 and 10 μm were clearly distinguished for PLA/PAni, whereas the diameter variability of neat PLA fibers was from 1.2 to ∼3 μm only. In spite of such notable variability, the distribution profiles of PLA/PAni fibers show a predominant size of 3−5 μm, independently of the CP concentration. It is worth noting that the average diameter of the fibers increases with the PAni concentration in the electrospinning mixture (i.e., values progressively increase from 3.5 to 5.2 μm when the PAni content grows from 2.5 to 10% w/w). The opposite effect was observed for fibers prepared using a mixture of PLA and poly(3-thiophene methyl acetate), a soluble PTh derivative, for which a slight reduction of the average diameter was detected.[66]

Because of the affinity of PEG toward chloroform, which is stronger than that of PLA, and its plasticizing effect, electrospun PLA/PEG/PAni fibers were prepared as described in the Methods section (Table 1). The addition of a small fraction of PEG to the feeding solution resulted in the achievement of a denser packing of the PLA and PAni chains through microphase segregation between PLA and PEG.[31] Representative SEM micrographs and diameter distribution of PLA/PEG-0.1/PAni and PLA/PEG-0.3/PAni fibers are displayed in Figure 2a. Although PLA/PEG/PAni fibers maintain a cylindrical shape and texture observed for PLA/PAni-5%, independently of the PEG content, the diameter experiences a drastic reduction (i.e., about half), which has been attributed to the plasticizer effect of PEG. Thus, the diameter of PLA/PEG/PAni fibers is 2.3−2.4 μm, whereas the diameter of PLA/PAni-5% is around 4 μm. These observations confirm that the packing of PLA chains undergoes a significant enhancement upon the incorporation of a small fraction of PEG to the feeding mixture.

The main structural characteristics of the fibers were maintained after removal of PEG from PLA/PEG/PAni fibers by solvent etching using water. This is evidenced in Figure 2b, which compares the morphology, texture, and diameter of PLA-0.3/PAni and PLA-0.1/PAni. The shape and texture of the fibers did not experience any significant change with respect to PLA/PEG/PAni fibers, whereas the diameter reduced by ∼0.2 μm after the selective etching process. The lack of holes in the surface of PLA-0.3/PAni and PLA-0.1/PAni fibers suggests that PEG was organized in nanodomains in the corresponding PLA/PEG/PAni fibers. This hypothesis is supported by root-mean-square (rms) roughness measurements, which were conducted by profilometry. Thus, the roughness of PLA-0.3/PAni and PLA-0.1/PAni fibers (R_q = 138 ± 23 and 103 ± 21 nm, respectively) was similar to that of PLA/PEG-0.3/PAni and PLA/PEG-0.1/PAni (R_q = 149 ± 41 and 116 ± 22 nm, respectively).

Core−shell PLA//PLA/PAni and PLA/PEG//PLA/PAni fibers, which were obtained using the operating conditions optimized for uniaxial fibers, are displayed in Figure 3a. As it can be seen, undesirable beads were formed in all cases. The

DOI: 10.1021/acsomega.8b03411
ACS Omega 2019, 4, 3660−3672

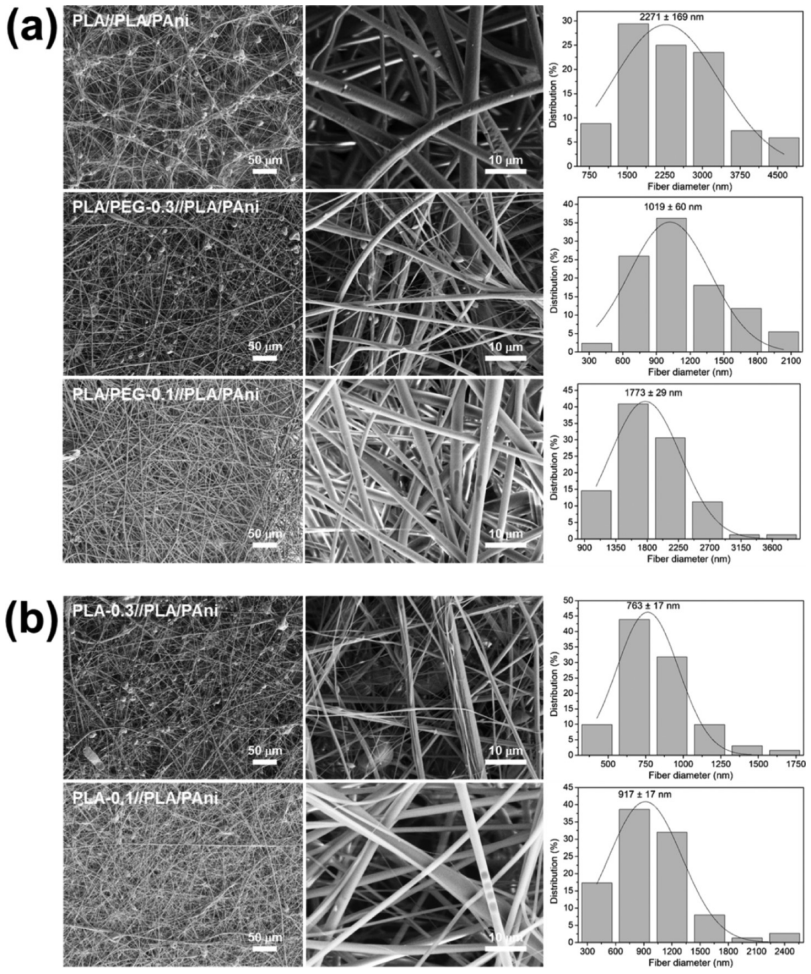

Figure 3. SEM micrographs taken at low (left) and high (center) magnification for electrospun fibers of (a) PLA//PLA/PAni, PLA/PEG-0.3//PLA/PAni and PLA/PEG-0.1//PLA/PAni; (b) PLA-0.3//PLA/PAni and PLA-0.1//PLA/PAni. The diameter distribution of the electrospun microfibers is displayed at the right.

formation of these structural defects has been attributed to the fact that the combination of mixtures of polymers increases the surface tension favoring the solidification of droplets into beads supported on fibers.[67] The number of beads decreased considerably for PLA/PEG-0.1//PLA/PAni, suggesting that the integration between the shell and the PAni-containing core becomes easier when a small amount of PEG is incorporated into the shell electrospinning solution. Most importantly, the diameter of the fibers decreases upon the incorporation of PEG in comparison with PLA//PLA/PAni (i.e., 0.5 and 1.0 μm for PLA/PEG-0.1//PLA/PAni and PLA/PEG-0.3//PLA/PAni, respectively). This is consistent with the enhancement of the packing of the PLA chains at the core. Core−shell fibers kept the structure after etching the PEG (Figure 3b), even though the average diameter reduced at the sub-micrometric scale.

Representative atomic force microscopy (AFM) topographic and phase-contrast images of PLA, PLA/PAni-5%, and PLA/PAni-10% fibers are compared in Figure 4. The fibers present a smooth surface and well-defined topography, the rms roughness being R_q = 11.6 ± 3.7, 17.4 ± 2.9, and 11.3 ± 0.6 nm, respectively. Phase-contrast images suggest that the CP is organized in nanoaggregates, which are identified by dark spots, very close to each other, probably forming conducting pathways.

Inspection of the cross section of fibers obtained by coaxial electrospinning using different microscopy techniques did not provide direct evidence about their core−shell structure. However, the thermal and electrical properties and, especially, the biological response of these fibers were very different to those of simple fibers (see below), suggesting that coaxial electrospinning led to the expected core−shell structure.

Spectroscopic Characterization of Electrospun Fibers. The Fourier-transform infrared spectroscopy (FTIR) spectrum of the as-prepared PAni/DBSA is displayed in Figure S1. The main bands, which are in agreement with those previously reported in the literature,[68,69] appear at 3450 cm^{-1} (N−H stretching), 2963 and 2924 cm^{-1} (aromatic C−H asymmetric stretching), 1547 and 1455 cm^{-1} (C═C stretching of quinoid and benzenoid ring, respectively), 1325 cm^{-1} (N−H bending), 1245 cm^{-1} (C−N stretching), and 1187 and 839 cm^{-1} (in-plane and out-of-plane C−H bending, respectively).

The FTIR spectra of PLA/PAni and neat PLA fibers are highly similar (Figure 5a) because of both the low content of PAni and the low intensity of the bands associated with its nonpolar and weakly polar groups. Therefore, the C═O stretching vibration at 1755 cm^{-1} and the asymmetric and symmetric C−O stretching at 1184 and 1086 cm^{-1}, respectively, are the more intense bands of PLA, whereas the signals of PAni/DBSA are identified as shoulders only. More specifically, the shoulders at 1258, 1558, and 2973 cm^{-1} have been attributed to the C−N stretching of primary aromatic amine, C═C stretching of the

DOI: 10.1021/acsomega.8b03411
ACS Omega 2019, 4, 3660−3672

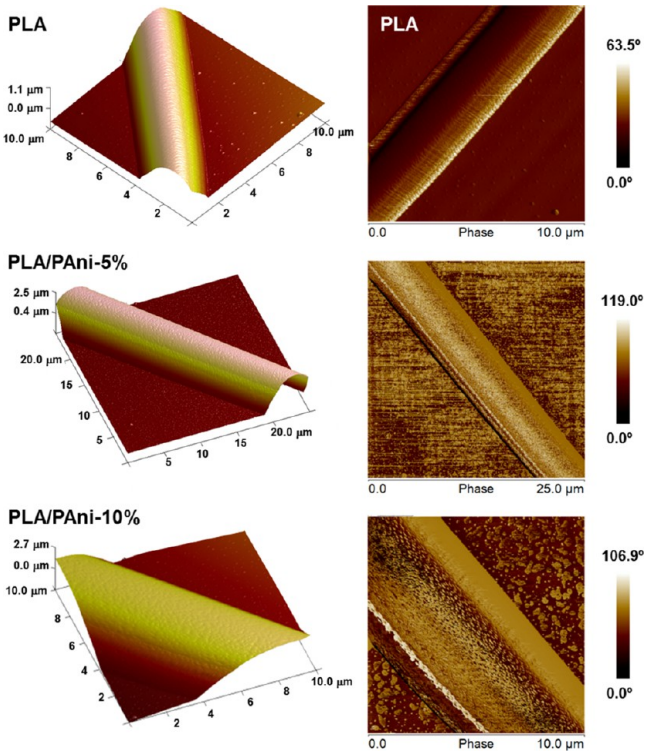

Figure 4. Representative topographic and phase-contrast AFM images (left and right, respectively) of PLA, PLA/PAni-5%, and PLA/PAni-10% electrospun fibers.

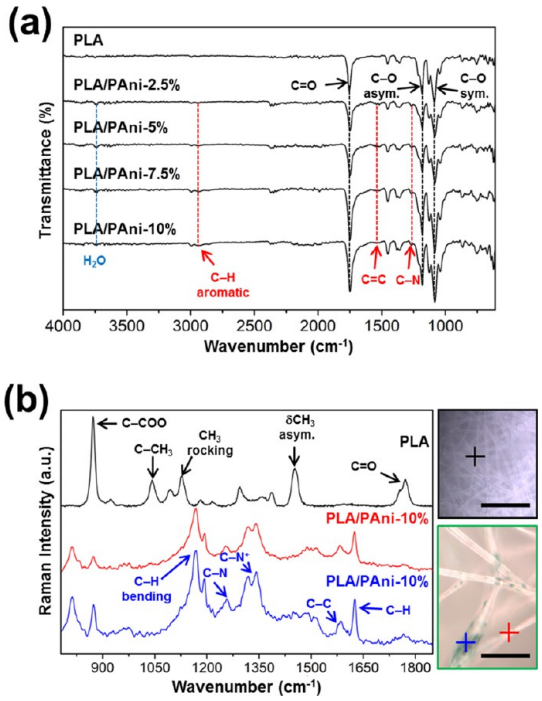

Figure 5. (a) FTIR spectra of PLA and PLA/PAni uniaxial fibers. The most important bands for PLA and PAni are indicated in black and red, respectively. (b) PLA and PLA/PAni-10% Raman spectra at the cross points in the optical images (scale bar: 50 μm).

ring, and aromatic C−H stretching, respectively. On the other hand, uniaxial PLA/PEG/PAni and core−shell PLA/PEG//PLA/PAni fibers (Figures S2 and S3, respectively) show almost the same absorption peaks as PLA/PAni, indicating that there is no bond formed or strong chemical interaction occurring within the blend. Thus, the most important difference is the apparition of the aliphatic C−H stretching band at 2855 cm^{-1}, which has been attributed to the PEG (i.e., many typical bands associated with PEG overlap with those of PLA).

Further studies were carried out to understand the compositional distribution of PLA/PAni fibers by means of micro-Raman spectroscopy. Figure 5b compares the Raman spectra and microscopy images of PLA and PLA/PAni-10% fibers. The most intense band in the PLA spectrum corresponds to the C−COO stretching and is located at 871 cm^{-1}. Other strong and medium peaks in the PLA Raman spectrum appear at 1755 and 1771 cm^{-1} (splitting patterns of C═O stretching), 1453 cm^{-1} (δCH_3 asymmetric mode), 1385 cm^{-1} (symmetric δCH_3 deformation), 1215 and 1095 cm^{-1} (asymmetric and symmetric C−O−C deformation, respectively), 1128 cm^{-1} (CH_3 rocking), and 1042 cm^{-1} (C−CH_3 stretching).[70]

Figure 5b displays the Raman spectra of two different spots of PLA/PAni-10% fibers using a source of 785 nm as exciting radiation. The spectrum recorded for the dark spot (blue line) has been associated with PAni/DBSA,[71,72] showing characteristic bands at 1193 cm^{-1} (C−H bending of the quinoid ring), 1257 (C−N stretching), 1318 and 1341 cm^{-1} (C−N^+ stretching), 1584 cm^{-1} (C−C stretching), and 1626 cm^{-1} (C−H stretching of the benzenoid ring). Among these bands, the intense overlapped ones at 1318 and 1341 cm^{-1} are particularly relevant as they are related with the C−N^+, stretching the modes of delocalized polaronic charge carriers, which is characteristic of the protonated imine form of PAni. The spectrum recorded for the second spot of the PLA/PAni-10%, which is located in the clearest area of the fiber (blue line), is also dominated by the CP signatures, evidencing that the scattering from PLA is very weak compared with that from PAni/DBSA. However, the change in the intensity of the bands in the spectra recorded for the two spots is consistent with the formation of interactions between PLA and PAni chains.

Inspection of the Raman spectra recorded for uniaxial PLA/PEG-0.3/PAni and core−shell PLA/PEG-0.3//PLA/PAni fibers, which are compared in Figure S4, indicates that the bands of PAni also dominate in the presence of PEG. The predominance of the PAni bands in blends with insulating polymers is due to the resonance Raman effect, which increases the intensity of the bands of the material when the laser energy coincides with the frequency of the electronic transition of the sample.[73,74] In blends of PAni with PLA and PEG, only the former absorbs in the wavelength of the employed exciting radiation, the intensities of its bands being enhanced with respect to those of insulating polymers.

Thermal, Electrical, and Mechanical Characterization. Differential scanning calorimetry (DSC) was employed to characterize thermal properties of PLA and PLA/PAni microfiber mats, and the results are displayed in Figure 6a. The DSC heating thermogram recorded for PLA indicates that the glass temperature, T_g, at 64 °C is followed by a broad exothermic peak corresponding to the cold polymer crystallization, which is consistent with the high molecular orientation attained in the electrospinning process,[74] and a sharp melting peak, T_m, at 168 °C also appears. The melting enthalpy is higher than the crystallization enthalpy (ΔH_m = 26.4 J/g and ΔH_c = 11.6 J/g), proving that some fraction of PLA was able to crystallize during the electrospinning process. All PLA/PAni samples show a clear glass transition, as could be presumed for amorphous samples, and a typical relaxation endothermic peak, which indicates that

DOI: 10.1021/acsomega.8b03411
ACS Omega 2019, 4, 3660−3672

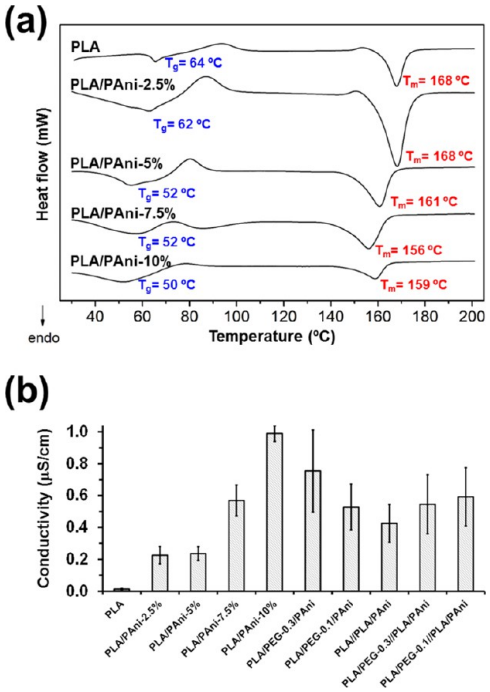

Figure 6. (a) DSC heating traces of PLA and PLA/PAni fibers. The glass transition and melting temperatures (T_g and T_m, respectively) are indicated. (b) Electrical conductivity of PLA, PLA/PAni, PLA/PEG/PAni, PLA//PLA/PAni, and PLA/PEG//PLA/PAni fibrous mats.

metastable PLA glassy material achieves equilibrium thermodynamic conditions with lower specific volume, enthalpy, and entropy. The concentration of CP in PLA/PAni blends has a remarkable influence on the characteristic T_g and T_m, especially when the content of PAni is ≥5% w/w (Table 2). Thus, the T_g

Table 2. Calorimetric Data of Uniaxial PLA/PAni and PLA/PEG/PAni Fibers and Core−Shell PLA//PLA/PAni and PLA/PEG//PLA/PAni Fibers

	T_g (°C)	T_m (°C)	ΔH_c (J/g)	ΔH_m (J/g)
PLA	64.3	167.9	11.6	26.4
PLA/PAni-2.5%	61.7	168.3	11.7	42.6
PLA/PAni-5%	52.0	160.6	8.4	27.9
PLA/PAni-7.5%	52.3	156.0	6.5	29.3
PLA/PAni-10%	49.9	158.8	4.0	15.8
PLA/PEG-0.3/PAni	50.7	166.7	13.5	39.3
PLA/PEG-0.1/PAni	56.1	167.5	2.8	29.2
PLA//PLA/PAni	61.2	166.6	16.1	50.3
PLA/PEG-0.3//PLA/PAni	49.5	167.6	6.6	51.7
PLA/PEG-0.1//PLA/PAni	51.6	168.0	10.2	30.3

and T_m decrease 12 and 9 °C, respectively, when the content of PAni in PLA fibers increases from 2.5 to 10% w/w. These observations are consistent with the DSC results for PAni/DBSA, which exhibited a T_g as low as 14 °C (Figure S5).

Comparison of PLA with PLA/PEG/PAni fibers (Figure S6 and Table 2) reveals similar features. Interestingly, the uniaxial fibers with the lowest PEG content, PLA/PEG-0.1/PAni, experienced the largest reduction in the T_g (13 °C) with respect to PLA, indicating that the former polymer acts as a plasticizer. This effect becomes more apparent with increasing PEG content. Comparison of core−shell PLA//PLA/PAni and PLA/PEG//PLA/PAni fibers (Figure S7 and Table 2) revealed that the incorporation of PEG at the shell causes a reduction of 9−11 °C, depending on the concentration. Overall, calorimetric results show that the T_m remains at ∼167 °C independently of the fibers' composition and architecture, whereas such parameters cause a reduction in the T_g of up to 14.8 °C with respect to PLA.

Electrical conductivities of all uniaxial and core−shell fibrous mats are compared in Figure 6b. The conductivity of PLA/PAni fibers increases with the amount of conduction paths, which grow with the content of CP. In spite of this, such increment is not particularly noticeable (i.e., from 0.23 ± 0.05 μS/cm for PLA/PAni-2.5% to 0.99 ± 0.05 μS/cm for PLA/PAni-10%). Unfortunately, determination of the electrical conductivity of PAni/DBSA was not possible as the CP films prepared for this purpose were extremely brittle. On the other hand, the incorporation of PEG to the microfibers results in a slight increment of the conductivity (i.e., from 0.24 ± 0.04 μS/cm for PLA/PAni-5% to 0.53 ± 0.14 μS/cm for PLA/PEG-0.1/PAni). This feature suggests that the enhancement of the PLA packing induced by the microphase segregation between PLA and PEG facilitates the interaction among neighboring CP chains and, therefore, the improvement of conduction paths. This hypothesis is consistent with the increment of the conductivity with the PEG content. Finally, the conductivity of the core−shell fibrous mats is similar (i.e., ∼0.5 μS) in all cases. Thus, although fibers prepared by coaxial electrospinning present different shell compositions, the content of PAni in the core was kept at 5% w/w.

The mechanical properties of PLA, PLA/PAni-5%, and PLA//PLA/PAni electrospun fibers, which have been chosen as representative because of their subsequent utilization in functional studies using cardiac cells (see below), have been evaluated and the results are displayed in Table 3. It is found that

Table 3. Results of the Stress−Strain Tests of Selected Electrospun Fibrous Mats

	Young's modulus (MPa)	strength (MPa)	failure strain (%)
PLA	44 ± 5	2.3 ± 0.7	51 ± 9
PLA/PAni-5%	31 ± 4	2.1 ± 0.4	32 ± 5
PLA//PLA/PAni	39 ± 3	2.2 ± 0.8	41 ± 7

Young's modulus and the strength of electrospun fiber mats are much lower compared with bulk PLA (∼3.5 GPa), which has been attributed to the combined effects of the porosity of the mats and the lack of orientation of the fibers. Besides, PLA mats display a slightly higher Young's modulus than PAni-containing systems, which is presumably due to its higher crystallinity as well as to the poor mechanical integrity of PAni. Also, PAni-containing systems exhibit a slightly lower failure strain, which may be explained by their heterogeneous structure in comparison with PLA.

PAni/DBSA Cytotoxicity. The cytotoxicity induced by the increasing concentration of PAni/DBSA in NRK, MCF-7, and MG-63 cells was estimated using the 3-(4,5-dimethylthiazol-2-yl)-2,5-diphenyltetrazolium bromide (MTT) test, which is based on measuring the viability of cells under treatment in comparison with untreated controls. The dose response curves, which are compared in Figure 7a, indicate that exposition to very low concentrations of PAni/DBSA (i.e., <0.01% w/w) does not cause serious toxicity, even though the harmful effects induced by this CP increases very rapidly. The cytotoxicity curves exhibit

DOI: 10.1021/acsomega.8b03411
ACS Omega 2019, 4, 3660−3672

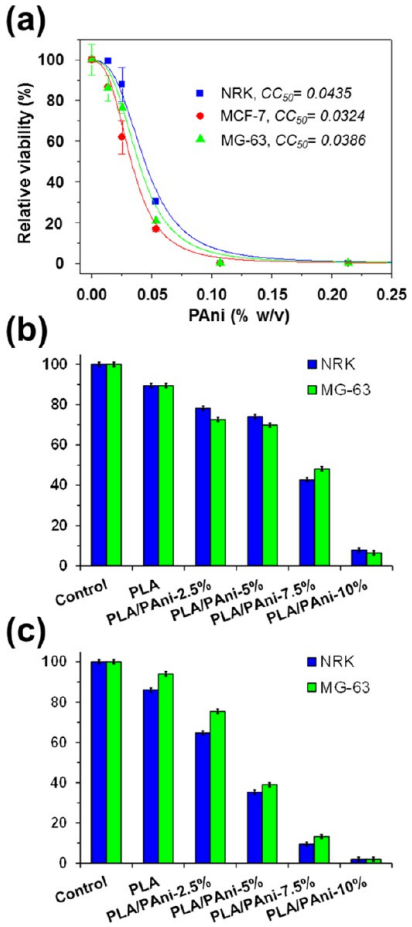

Figure 7. (a) Cytotoxicity curve of PAni/DBSA for NRK, MCF-7, and MG-63 cells. (b,c) Biocompatibility of PLA/PAni fibers expressed as relative viability of NRK and MG-63 culture cells onto the fibrous mats after (b) 24 h (cell adhesion) and (c) 96 h (cell proliferation).

a similar shape in all cases, indicating that the CP uses a single mechanism to kill the cells, independently of the cell line. Although the study of such mechanism is not within the scope of this work, previous studies[16] suggested that, after entering into the cytoplasm, PAni contacts the mitochondria, increasing its membrane porosity and unbalancing the electrolytes inside. Thus, PAni-induced alteration of the mitochondrial function could probably interrupt the respiratory chain. On the other hand, the half cytotoxic concentration (CC_{50}) of PAni/DBSA is comprised between 0.03 and 0.04% w/w (Figure 7a), which actually is a very low CP concentration.

On the basis of these results, the biocompatibility of PLA/PAni fibers has been tested by examining the adhesion and proliferation of cultured NRK and MG-63 cells on fibrous mats with growing PAni content. Thus, cell adhesion evaluates cytotoxicity as an early event, whereas cell proliferation evaluates a chronic effect of prolonged cytotoxicity. Figure 7b shows the percentage of cells that have adhered after 24 h in culture. The adhesion on PLA films decreases upon the incorporation of PAni, even though such reduction is only 11−20% on PLA/PAni-2.5% and PLA/PAni-5%. The adhesion decreases by more than 45 and 80% in fibers with 7.5 and 10% w/w of PAni, respectively. Cell proliferation, which was determined by evaluating the cell viability after 96 h, exhibits a drastic dependence of the PAni-content in the fibers (Figure 7c). Thus, the cell viability on PLA/PAni-2.5, -5, -7.5, and 10% decreases by around 20, 50, 80, and 90%, respectively, after such time interval.

Figure 7b,c reflects a clear dose-dependent effect of PAni on the biocompatibility of PLA/PAni fibers. Comparison of these results with the cytotoxicity curve displayed in Figure 7a indicates that, although PAni mainly remains inside the prepared fibers, a small fraction is released to the cell culture medium. For example, if a complete release is assumed, the content of CP in 1 mL of cell culture medium should be estimated to be around 0.12−0.15% w/w when a ∼20 mg of PLA/PAni-7.5% is maintained inside. According to Figure 7a, such concentration of PAni is high enough to kill 100% of the cell population exposed to the fibrous mat sample. However, Figure 7b shows that the cellular mortality is ∼55% after 24 h, which corresponds to 0.03−0.04% w/w PAni in the cytotoxicity curve. This feature reveals a release of 20−25% of the CP loaded into PLA/PAni-7.5% fibers. Similar results are obtained for the rest of PLA/PAni fibers, suggesting that attractive PLA···PAni interactions are responsible for the retention of the CP inside the matrix (i.e., otherwise, a total cell mortality should be immediately observed). Moreover, such intermolecular interactions persist for a long time as the fraction of surviving cells after 96 h is ∼10%.

Incorporation of biocompatible PEG into PAni-containing uniaxial fibers resulted in an increment of the cell mortality. This effect, which is reflected in Figure 8a,b for cell adhesion and cell

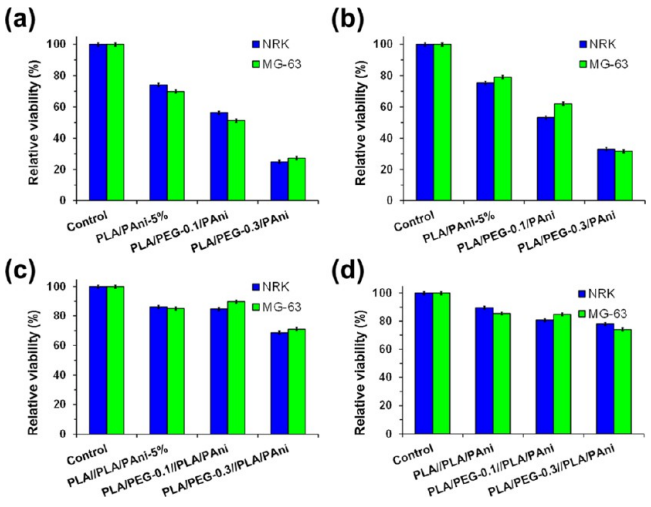

Figure 8. Biocompatibility of (a,b) PLA/PEG/PAni and (c,d) PLA/PEG//PLA/PAni fibers expressed as relative viability of NRK and MG-63 culture cells onto the fibrous mats after (a,c) 24 h (cell adhesion) and (b,d) 96 h (cell proliferation).

proliferation, respectively, grows with the content of PEG in the feeding PLA/PEG/PAni mixture. This behavior has been attributed to the remarkable PEG hydrophilicity, which rapidly dissolves into the culture medium, enhancing the porosity of the fibers and, therefore, favoring the release of PAni to the culture medium. As a consequence, the cell viability after both 24 and 96 h is ∼45% smaller for PLA/PEG-0.3/PAni than for PLA/PAni-5% (Figure 8a,b).

The incorporation of the shell at the PLA/PAni-5% core improves significantly the biocompatibility of the fibers. This is reflected in Figure 8c,d, which compares the cell adhesion and proliferation, respectively, for PLA//PLA/PAni PLA/PEG-0.3//PLA/PAni and PLA/PEG-0.1//PLA/PAni. As it can be seen, core−shell fibers exhibit higher biocompatibility than

DOI: 10.1021/acsomega.8b03411
ACS Omega 2019, 4, 3660−3672

uniaxial fibers in all cases, indicating that the shell exerts a notable control on the release of PAni from the core. Considering that PEG solubilizes in the culture medium, results displayed in Figure 8c,d evidence that the PAni release is mainly regulated by the porosity of the core, even though the shell also has some influence. Thus, cell viabilities are ∼10−15% lower for PLA/PEG-0.3//PLA/PAni than for PLA//PLA/PAni and PLA/PEG-0.1//PLA/PAni, showing that the biocompatibility decreases with the porosity of the shell.

Cardiac Cells on PLA/PAni-5% and PLA//PLA/PAni Fibrous Mats. The biocompatibility of PLA/PAni-5% and PLA//PLA/PAni materials on cardiac cells was evaluated using cardiac primary cells isolated from neonatal mice hearts. Cardiac fibroblasts were seeded on PLA (control) and PLA/PAni-5% uniaxial fibers and PLA//PLA/PAni coaxial fibers and a live/death assay was performed after 48 h of culture (Figure 9a).

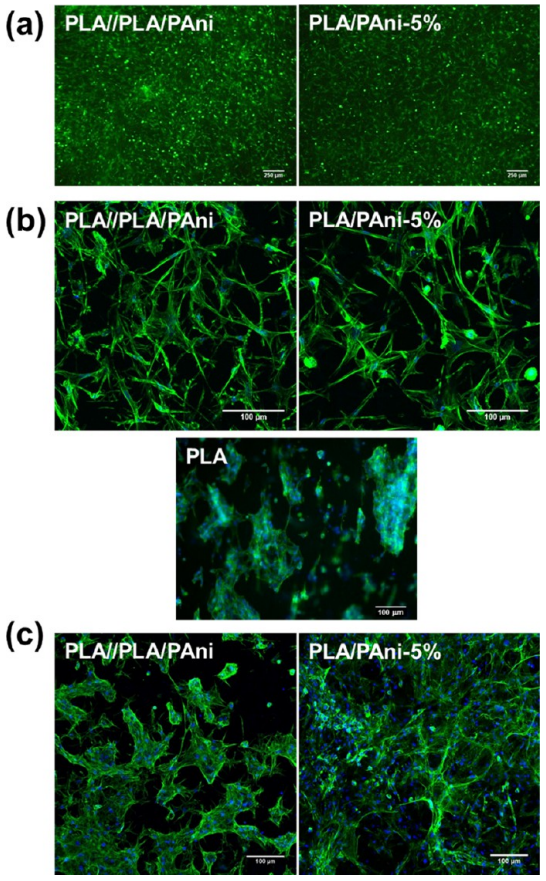

Figure 9. (a) Live/death assay of cardiac fibroblasts cultured on PLA//PLA/PAni coaxial and PLA/PAni-5% uniaxial fibers for 48 h (green: living cells; red: dead cells). (b,c) Confocal images of cardiac fibroblasts (b) and cardiomyocyte-enriched population (c) seeded on PLA//PLA/PAni coaxial fibers and PLA/PAni-5% and PLA (control) uniaxial fibers after 48 h and 13 days of incubation, respectively (green: phalloidin; blue: DAPI).

Cardiac fibroblasts were perfectly able to attach to the fibers and almost any dead cell could be detected after 48 h. This result evidenced again the biocompatibility observed before for these PLA- and PAni-containing fibers, which is due to the retention of the CP within PLA fibers through PAni···PLA interactions. Moreover, cardiac fibroblasts exhibited a high affinity toward PLA, PLA/PAni-5%, and PLA//PLA/PAni fibers where cells showed an elongated morphology, adapting their actin cytoskeleton to the material matrix (Figure 9b).

A cardiomyocyte-enriched population of cells was also used for the evaluation of the biocompatibility and suitability of PLA/PAni-5% and PLA//PLA/PAni fibrous mats for cardiac tissue engineering. After 7 days of incubation, cardiomyocytes still maintain their ability to beat on the fibers (Videos 1 and 2 display cardiomyocytes incubated on uniaxial PLA/PAni-5% and coaxial PLA//PLA/PAni fibers for 7 days), indicating that PLA/PAni-5% and PLA//PLA/PAni fibers are not only nontoxic to cardiac cells, but they also do not impede the normal cardiomyocyte functions and contractibility. In contrast, no beating activity was detected for cardiomyocytes adhered to control PLA fibers, reflecting that the electroactivity of PAni favors the functionality of cardiac cells. On the other hand, cardiomyocytes showed good adherence and survival after 13 days of culture on these mats, both uniaxial and coaxial (Figure 9c), being even able to colonize the material matrix with high interconnectivity between cells.

CONCLUSIONS

Simple PLA, PLA/PAni, and PLA/PEG/PAni fibers and core−shell PLA/PLA/PAni and PLA/PEG//PLA/PAni fibers have been successfully prepared by uniaxial and coaxial electrospinning, respectively. The diameter of the uniaxial fibers increases with the PAni content, whereas it decreases upon the addition of PEG to the feeding mixture. This reduction, which is maintained after selective PEG etching, has been attributed to the microphase segregation between PLA and PEG that induces a denser packing of PLA and PAni chains. This effect is preserved in core−shell PLA/PEG//PLA/PAni fibers. The glass transition and melting temperatures of PLA/PAni fibers decrease with increasing concentration of PAni, whereas the addition of PEG only affects the glass transition. Besides, the electrical conductivity of the fibers increases with the PAni content, as it was expected, and with the PEG content, which has been attributed to the enhancement of PAni···PAni interactions.

Although PAni/DBSA has been found to be cytotoxic, this harmful effect is significantly reduced in PLA/PAni fibers as the formation of favorable PLA···PAni interactions avoids the release of the CP from the fiber. Amazingly, the incorporation of PEG to uniaxial fibers causes the opposite effect, reducing the biocompatibility of the fibers. However, the biocompatibility of core−shell fibers is higher than that of uniaxial fibers. Finally, the proposed PLA/PAni-5% uniaxial and PLA//PLA/PAni coaxial fibers have demonstrated their suitability for cardiac tissue engineering, overcoming the abovementioned toxicity of the CP. The material offers very good adhesion for cardiac cells, also being able to modulate cell shape and orientation, something important for the characteristic anisotropy of the cardiac tissue. The investigated fibers do not induce interferences or impediments for the developing of the beating and contraction functions of cardiomyocytes, supporting their promising applicability in cardiac tissue engineering and the developing of cardiac grafts.

METHODS

Materials. Aniline monomer (Neon Comercial Ltda) was previously distilled and stored under refrigeration. DBSA (Nacure 5076, King Industries), ammonium persulfate (APS; Neon Comercial Ltda), and toluene (Neon Comercial Ltda;

DOI: 10.1021/acsomega.8b03411
ACS Omega 2019, 4, 3660−3672

solvent reagent grade) were used without further purification. Distilled water was used for the emulsion polymerization.

PLA, a product of NatureWorks (polymer 3001D), was kindly supplied by Nupik International (Polinyà, Spain). According to the manufacturer, this PLA has a *D* content of ∼1.5%, a residual monomer content of 0.3%, density of 1.24 g/cm^3, glass transition temperature of T_g = 55−60 °C, and melting point of T_m = 155−170 °C. The number and weight average molecular weights and polydispersity index, as determined by gel permeation chromatography, were M_n = 98 100 g/mol, M_w = 181 000 g/mol and 1.85, respectively. PEG samples of M_n = 35 000 g/mol, acetonitrile, and chloroform (analytical reagent grade) were purchased from Sigma-Aldrich.

Synthesis of PAni. PAni doped with DBSA, hereafter PAni/DBSA, was obtained using a previously described procedure.[75] Specific details are provided in the Supporting Information.

Electrospun Uniaxial and Coaxial Fibers. Control PLA fibers were electrospun from chloroform/acetone (2:1 v/v) at a polymer concentration of 16.6% w/v. For uniaxial PLA/PAni fiber preparation, PLA/PAni mixtures with 2.5−10% w/w PAni (relative to PLA) were dissolved in chloroform at a polymer concentration of 16.6% w/v. Hereafter, PLA/PAni samples will be identified indicating the PAni weight percentage ratio (e.g., PLA/PAni-5% corresponds to a mixture with 5% w/w of PAni relative to PLA). For the preparation of uniaxial PLA/PEG/PAni fibers, PLA/PEG mixtures with 0.7:0.3 and 0.9:0.1 w/w ratios were dissolved in chloroform at a polymer concentration of 16.6% w/v, whereas the PAni concentration was maintained at 5% w/w (relative to PLA/PEG). Samples will be identified indicating the PEG fraction in the PLA/PEG mixture (e.g., PLA/PEG-0.3/PAni corresponds to a 0.7:0.3 w/w PLA/PEG mixture with 5% w/w of PAni relative to PLA/PEG). After this, the PEG was etched from PLA/PEG/PAni fibers using water. For this purpose, the fibers were kept submerged for 24 h. After PEG elimination, the resulting PLA/PAni fibers will be identified maintaining the PEG's fraction from the initial feeding mixture (e.g., PLA-0.3/PAni corresponds to the fibers obtained by dissolving the PEG molecules of PLA/PEG-0.3/PAni).

Coaxial electrospinning was performed by varying the composition of the polymer mixtures used for the shell. These were PLA and PLA/PEG (0.7:0.3 and 0.9:0.1 w/w PLA/PEG) in chloroform at a polymer concentration of 8.3% w/v. The core was electrospun using a PLA/PAni mixture with 5% w/w of PAni (relative to PLA) dissolved in chloroform at a polymer concentration of 8.3% w/v. The code used to denote coaxial fibers refers to the composition of the solutions used for the shell//core (e.g., PLA/PEG-0.3//PLA/PAni indicates that the shell was electrospun using a 0.7:0.3 w/w PLA/PEG mixture whereas the core comes from a PLA/PAni mixture with 5% w/w-of PAni relative to PLA). As described above for uniaxial PLA/PEG/PAni fibers, PEG was etched from PLA/PEG//PLA/PAni coaxial fibers using water. Table 1 summarizes the nomenclature and composition of all fibers prepared in this work.

Operating conditions were optimized for PLA/PAni and PLA//PLA/PAni fibers and, subsequently, used to produce the PLA/PEG/PAni and PLA/PEG//PLA/PAni ones. The solutions were mixed and loaded in a 5 mL BD (Becton Dickinson Co., Franklin Lakes, NJ, USA) plastic syringe for delivery through an 18 G needle tip (inside diameter 0.84 mm) at a mass-flow rate of 5 mL/h for uniaxial electrospinning, and through a coaxial system with 14 G (shell) and 21 G (core) needles (inside diameter of 1.6 and 0.8 mm, respectively) at a mass-flow rate of 1.2 mL/h for coaxial electrospinning, using a KDS100 infusion pump (KD Scientific, USA). The voltage, which was applied through a high-voltage Gamma High Voltage Research (ES30-5W) power supply, was 15 kV for PLA, PLA/PAni, and PLA/PEG/PAni fibers, increasing to 20 kV for PLA//PLA/PAni and PLA/PEG//PLA/PAni ones. All electrospun fibers were obtained using a needle tip-collector distance of 25 cm. All electrospinning experiments were carried out at room temperature.

Characterization. Characterization was carried out using SEM, AFM, FTIR, and micro-Raman spectroscopies, DSC, and electrical measurements. Details are provided in the Supporting Information.

Cytotoxicity. Cellular assays were performed using normal rat fibroblasts (NRK) and epithelial cells derived from breast adenocarcinoma (MCF-7) and osteosarcoma (MG-63). Cells were cultured in Dulbecco's modified Eagle's medium (DMEM) with 4500 mg of glucose/L and supplemented with 10% fetal bovine serum (FBS), penicillin (100 units/mL), and streptomycin (100 μg/mL). The cultures were maintained in a humidified incubator with an atmosphere of 5% CO_2 and 95% O_2 at 37 °C. Culture media were changed every 2 days. When cells reached 80−90% confluence, they were detached using 1−2 mL of trypsin [0.25% trypsin/ethylenediaminetetraacetic acid (EDTA)] for 5 min at 37 °C. Finally, cells were re-suspended in 5 mL of fresh medium and their concentration was determined with a Neubauer camera using 0.4% trypan blue.

Fiber mats were placed in plates of 24 wells, adhered with a small drop of silicone (Silbione MED ADH 4300 RTV, Bluestar Silicones France SAS, Lyon, France), and sterilized using UV irradiation for 15 min in a laminar flux cabinet. An aliquot of 50 μL containing 5×10^4 and 2×10^4 cells was deposited on the film surface at each well for adhesion and proliferation assays, respectively. Bare steel sheets were used as controls. Attachment of the cells was promoted by incubation under culture conditions for 30 min. Finally, 1 mL of the culture medium was added to each well. In order to evaluate cell viability after 24 and 96 h, colorimetric MTT assays were conducted. Specifically, 50 μL of MTT solution [5 mg/mL in phosphate buffered saline (PBS)] was added to each well. After 3 h of incubation, samples were washed twice with PBS and stored in clean wells. In order to dissolve the formed formazan crystals, 0.5 mL of dimethyl sulfoxide/methanol/water (70/20/10% v/v) was added. Finally, the absorbance was measured in a plate reader at 570 mm using 200 μL of dissolution. Viability results derived from the average of five replicates (n = 5) for each independent experiment were normalized to tissue culture polystyrene as relative percentages (control).

Cardiac Cell Viability and Adhesion. Cardiac primary cells were obtained from CD1 neonatal mouse following a series of enzymatic digestions. Briefly, hearts from 1 to 3 day-old mice were extracted, cleaned, and minced into small pieces using curved scissors. Tissue fragments underwent a predigestion step by incubating in trypsin/EDTA solution 0.25% with 4 μg/mL DNase I and subjected to 20−25 cycles of enzymatic digestion using collagenase II and dispase II in L-15 medium. Pooled supernatants were collected through a 70 μm nylon cell strainer and the pellet was resuspended in DMEM containing 1 g/L glucose supplemented with 19% M-199 medium, 10% horse serum, 5% FBS, and 1% penicillin and streptomycin. The cell suspension was plated into a 10 cm cell culture dish in order to separate the non-myocytic cell fraction of the heart, mainly

DOI: 10.1021/acsomega.8b03411
ACS Omega 2019, 4, 3660−3672

fibroblasts, and obtain an enriched population of cardiomyocytes.

Fibers mats were placed in 24-well plates, fixed using Teflon rings and sterilized by UV irradiation for 15 min in a laminar flux cabinet. Cardiac fibroblasts and cardiomyocytes were seeded and culture on fiber mats for the indicated time at 37 °C and 5% CO_2. Culture media were replaced every 2−3 days. Incubation with calcein-AM and propidium iodide for 20 min was employed for live/death assay. For cell morphology observation, cardiac cells were fixed in paraformaldehyde 4% solution and stained with Acti-stain 488 phalloidin and 4′,6-diamidino-2-phenylindole (DAPI) for the actin cytoskeleton and nucleus visualization, respectively. Fluorescence images were taken using a Confocal Microscope LSM 800 (Zeiss). The beating analysis was performed using an inverted microscope Leica DM IL LED. The videos were recorded at 19 fps with a 1024 × 768 pixel resolution.

■ ASSOCIATED CONTENT

Supporting Information

The Supporting Information is available free of charge on the ACS Publications website at DOI: 10.1021/acsomega.8b03411.

Cardiomyocytes incubated on uniaxial PLA/PAni-5% fibers (AVI)

Experimental methods, FTIR and Raman spectra, and DSC heating scans (PDF)

Cardiomyocytes incubated on coaxial PLA//PLA/PAni (AVI)

■ AUTHOR INFORMATION

Corresponding Authors

*E-mail: eengel@ibecbarcelona.eu (E.E.).
*E-mail: luis.javier.del.valle@upc.edu (L.J.d.V.).
*E-mail: carlos.aleman@upc.edu (C.A.).

ORCID

Elaine Armelin: 0000-0002-0658-7696
Elisabeth Engel: 0000-0003-4855-8874
Carlos Alemán: 0000-0003-4462-6075

Notes

The authors declare no competing financial interest.

■ ACKNOWLEDGMENTS

The authors acknowledge MINECO/FEDER (MAT2015-69367-R, MAT2015-69547-R, MAT2015-62725-ERC, and MAT2015-68906-R), EUIN73, and the Agència de Gestió d'Ajuts Universitaris i de Recerca (2017SGR359) for financial support and the Brazilian government agency CAPES (process PDSE: 88881.133689/2016-01), which provided the financial support for scholarship. Support for the research of C.A. was received through the prize "ICREA Academia" for excellence in research funded by the Generalitat de Catalunya. We acknowledge Lourdes Sanchez for her help in animal caring and hearts' extraction.

■ REFERENCES

(1) Smith, A. S. T.; Yoo, H.; Yi, H.; Ahn, E. H.; Lee, J. H.; Shao, G.; Nagornyak, E.; Laflamme, M. A.; Murry, C. E.; Kim, D.-H. Micro- and Nano-Patterned Conductive Graphene−PEG Hybrid Scaffolds for Cardiac Tissue Engineering. *Chem. Commun.* **2017**, *53*, 7412−7415.

(2) Thompson, B. C.; Murray, E.; Wallace, G. G. Graphite Oxide to Graphene. Biomaterials to Bionics. *Adv. Mater.* **2015**, *27*, 7563−7582.

(3) Encabo-Berzosa, M. d. M.; Sancho-Albero, M.; Crespo, A.; Andreu, V.; Sebastian, V.; Irusta, S.; Arruebo, M.; Martín-Duque, P.; Santamaria, J. The Effect of PEGylated Hollow Gold Nanoparticles on Stem Cell Migration: Potential Application in Tissue Regeneration. *Nanoscale* **2017**, *9*, 9848−9858.

(4) Ahadian, S.; Davenport Huyer, L.; Estili, M.; Yee, B.; Smith, N.; Xu, Z.; Sun, Y.; Radisic, M. Moldable Elastomeric Polyester-Carbon Nanotube Scaffolds for Cardiac Tissue Engineering. *Acta Biomater.* **2017**, *52*, 81−91.

(5) Guimard, N. K.; Gomez, N.; Schmidt, C. E. Conducting Polymers in Biomedical Engineering. *Prog. Polym. Sci.* **2007**, *32*, 876−921.

(6) Guo, B.; Glavas, L.; Albertsson, A.-C. Biodegradable and electrically conducting polymers for biomedical applications. *Prog. Polym. Sci.* **2013**, *38*, 1263−1286.

(7) Pérez-Madrigal, M. M.; Giannotti, M. I.; del Valle, L. J.; Franco, L.; Armelin, E.; Puiggalí, J.; Sanz, F.; Alemán, C. Thermoplastic Polyurethane:Polythiophene Nanomembranes for Biomedical and Biotechnological Applications. *ACS Appl. Mater. Interfaces* **2014**, *6*, 9719−9732.

(8) Pérez-Madrigal, M. M.; Armelin, E.; del Valle, L. J.; Estrany, F.; Alemán, C. Bioactive and Electroactive Response of Flexible Polythiophene:Polyester Nanomembranes for Tissue Engineering. *Polym. Chem.* **2012**, *3*, 979−981.

(9) Guo, B.; Ma, P. X. Conducting Polymers for Tissue Engineering. *Biomacromolecules* **2018**, *19*, 1764−1782.

(10) Zhao, X.; Guo, B.; Wu, H.; Liang, Y.; Ma, P. X. Injectable Antibacterial Conductive Nanocomposite Cryogels with Rapid Shape Recovery for Noncompressible Hemorrhage and Wound Healing. *Nat. Commun.* **2018**, *9*, 2784.

(11) Llorens, E.; Armelin, E.; Pérez-Madrigal, M. d. M.; del Valle, L.; Alemán, C.; Puiggalí, J. Nanomembranes and Nanofibers from Biodegradable Conducting Polymers. *Polymers* **2013**, *5*, 1115−1157.

(12) del Valle, L. J.; Aradilla, D.; Oliver, R.; Sepulcre, F.; Gamez, A.; Armelin, E.; Alemán, C.; Estrany, F. Cellular Adhesion and Proliferation on Poly(3,4-ethylenedioxythiophene): Benefits in the Electroactivity of the Conducting Polymer. *Eur. Polym. J.* **2007**, *43*, 2342−2349.

(13) George, P. M.; Lyckman, A. W.; LaVan, D. A.; Hegde, A.; Leung, Y.; Avasare, R.; Testa, C.; Alexander, P. M.; Langer, R.; Sur, M. Fabrication and Biocompatibility of Polypyrrole Implants Suitable for Neural Prosthetics. *Biomaterials* **2005**, *26*, 3511−3519.

(14) Fahlgren, A.; Bratengeier, C.; Gelmi, A.; Semeins, C. M.; Klein-Nulend, J.; Jager, E. W. H.; Bakker, A. D. Biocompatibility of Polypyrrole with Human Primary Osteoblasts and the Effect of Dopants. *PLoS One* **2015**, *10*, e0134023.

(15) Yang, B.; Yao, F.; Hao, T.; Fang, W.; Ye, L.; Zhang, Y.; Wang, Y.; Li, J.; Wang, C. Development of Electrically Conductive Double-Network Hydrogels via One-Step Facile Strategy for Cardiac Tissue Engineering. *Adv. Healthcare Mater.* **2016**, *5*, 474−488.

(16) Li, Y.-S.; Chen, B.-F.; Li, X.-J.; Zhang, W. K.; Tang, H.-B. Cytotoxicity of Polyaniline Nanomaterial on Rat Celiac Macrophages In Vitro. *PLoS One* **2014**, *9*, e107361.

(17) Villalba, P.; Ram, M. K.; Gomez, H.; Bhethanabotla, V.; Helms, M. N.; Kumar, A.; Kumar, A. Cellular and In Vitro Toxicity of Nanodiamond-Polyaniline Composites in Mammalian and Bacterial Cell. *Mater. Sci. Eng., C* **2012**, *32*, 594−598.

(18) Humpolicek, P.; Kasparkova, V.; Saha, P.; Stejskal, J. Biocompatibility of Polyaniline. *Synth. Met.* **2012**, *162*, 722−727.

(19) Kucekova, Z.; Humpolicek, P.; Kasparkova, V.; Perecko, T.; Lehocký, M.; Hauerlandová, I.; Sáha, P.; Stejskal, J. Colloidal Polyaniline Dispersions: Antibacterial Activity, Cytotoxicity and Neutrophil Oxidative Burst. *Colloids Surf., B* **2014**, *116*, 411−417.

(20) Bober, P.; Humpolíček, P.; Pacherník, J.; Stejskal, J.; Lindfors, T. Conducting Polyaniline Based Cell Culture Substrate for Embryonic Stem Cells and Embryoid Bodies. *RSC Adv.* **2015**, *5*, 50328−50335.

(21) MacDiarmid, A. G.; Epstein, A. J. Polyanilines: a novel class of conducting polymers. *Faraday Discuss.* **1989**, *88*, 317−332.

(22) *Polyaniline Blends, Composites, and Nanocomposites*; Vishakh, P. M.; Della Pina, C.; Falletta, E., Eds.; Elsevier: Amsterdam, Netherlands, 2018.

DOI: 10.1021/acsomega.8b03411
ACS Omega 2019, 4, 3660−3672

(23) Hans, M.; Shimoni, K.; Danino, D.; Siegel, S. J.; Lowman, A. Synthesis and Characterization of mPEG−PLA Prodrug Micelles. *Biomacromolecules* **2005**, *6*, 2708−2717.
(24) Pérez-Madrigal, M. M.; Armelin, E.; Puiggalí, J.; Alemán, C. Insulating and Semiconducting Polymeric Free-Standing Nanomembranes with Biomedical Applications. *J. Mater. Chem. B* **2015**, *3*, 5904−5932.
(25) Saini, P.; Arora, M.; Kumar, M. N. V. R. Poly(lactic acid) Blends in Biomedical Applications. *Adv. Drug Delivery Rev.* **2016**, *107*, 47−59.
(26) Li, Z.; Tan, B. H.; Lin, T.; He, C. Recent Advances in Stereocomplexation of Enantiomeric PLA-Based Copolymers and Applications. *Prog. Polym. Sci.* **2016**, *62*, 22−72.
(27) Nofar, M.; Park, C. B. Poly (lactic acid) foaming. *Prog. Polym. Sci.* **2014**, *39*, 1721−1741.
(28) Armentano, I.; Bitinis, N.; Fortunati, E.; Mattioli, S.; Rescignano, N.; Verdejo, R.; Lopez-Manchado, M. A.; Kenny, J. M. Multifunctional Nanostructured PLA Materials for Packaging and Tissue Engineering. *Prog. Polym. Sci.* **2013**, *38*, 1720−1747.
(29) Wang, Q.; He, W.; Huang, J.; Liu, S.; Wu, G.; Teng, W.; Wang, Q.; Dong, Y. Synthesis of Water Soluble, Biodegradable, and Electroactive Polysaccharide Crosslinker with Aldehyde and Carboxylic Groups for Biomedical Applications. *Macromol. Biosci.* **2011**, *11*, 362−372.
(30) Liu, Y.; Hu, J.; Zhuang, X.; Zhang, P.; Wei, Y.; Wang, X.; Chen, X. Synthesis and Characterization of Novel Biodegradable and Electroactive Hydrogel Based on Aniline Oligomer and Gelatin. *Macromol. Biosci.* **2012**, *12*, 241−250.
(31) Huang, L.; Zhuang, X.; Hu, J.; Lang, L.; Zhang, P.; Wang, Y.; Chen, X.; Wei, Y.; Jing, X. Synthesis of Biodegradable and Electroactive Multiblock Polylactide and Aniline Pentamer Copolymer for Tissue Engineering Applications. *Biomacromolecules* **2008**, *9*, 850−858.
(32) Huang, L.; Hu, J.; Lang, L.; Wang, X.; Zhang, P.; Jing, X.; Wang, X.; Chen, X.; Lelkes, P. I.; MacDiarmid, A. G.; Wei, Y. Synthesis and Characterization of Electroactive and Biodegradable ABA Block Copolymer of Polylactide and Aniline Pentamer. *Biomaterials* **2007**, *28*, 1741−1751.
(33) Guo, B.; Finne-Wistrand, A.; Albertsson, A.-C. Molecular Architecture of Electroactive and Biodegradable Copolymers Composed of Polylactide and Carboxyl-Capped Aniline Trimer. *Biomacromolecules* **2010**, *11*, 855−863.
(34) Xie, M.; Wang, L.; Guo, B.; Wang, Z.; Chen, Y. E.; Ma, P. X. Ductile Electroactive Biodegradable Hyperbranched Polylactide Copolymers Enhancing Myoblast Differentiation. *Biomaterials* **2015**, *71*, 158−167.
(35) Liu, Y.; Hu, J.; Zhuang, X.; Zhang, P.; Chen, X.; Wei, Y.; Wang, X. Preparation and Characterization of Biodegradable and Electroactive Polymer Blend Materials Based on mPEG/Tetraaniline and PLLA. *Macromol. Biosci.* **2011**, *11*, 806−813.
(36) Cui, H.; Shao, J.; Wang, Y.; Zhang, P.; Chen, X.; Wei, Y. PLA-PEG-PLA and Its Electroactive Tetraaniline Copolymer as Multiinteractive Injectable Hydrogels for Tissue Engineering. *Biomacromolecules* **2013**, *14*, 1904−1912.
(37) Guo, B.; Finne-Wistrand, A.; Albertsson, A.-C. Degradable and Electroactive Hydrogels with Tunable Electrical Conductivity and Swelling Behavior. *Chem. Mater.* **2011**, *23*, 1254−1262.
(38) Guo, B.; Finne-Wistrand, A.; Albertsson, A.-C. Electroactive Hydrophilic Polylactide Surface by Covalent Modification with Tetraaniline. *Macromolecules* **2012**, *45*, 652−659.
(39) Wu, Y.; Wang, L.; Guo, B.; Shao, Y.; Ma, P. X. Electroactive Biodegradable Polyurethane Significantly Enhanced Schwann Cells Myelin Gene Expression and Neurotrophin Secretion for Peripheral Nerve Tissue Engineering. *Biomaterials* **2016**, *87*, 18−31.
(40) Li, M.; Guo, Y.; Wei, Y.; MacDiarmid, A.; Lelkes, P. Electrospinning Polyaniline-Contained Gelatin Nanofibers for Tissue Engineering Applications. *Biomaterials* **2006**, *27*, 2705−2715.
(41) McKeon, K. D.; Lewis, A.; Freeman, J. W. Electrospun Poly(D,L-lactide) and Polyaniline Scaffold Characterization. *J. Appl. Polym. Sci.* **2010**, *115*, 1566−1572.
(42) Wang, L.; Wu, Y.; Hu, T.; Guo, B.; Ma, P. X. Electrospun conductive nanofibrous scaffolds for engineering cardiac tissue and 3D bioactuators. *Acta Biomater.* **2017**, *59*, 68−81.
(43) Zhao, X.; Li, P.; Guo, B.; Ma, P. X. Antibacterial and Conductive Injectable Hydrogels Based on Quaternized Chitosan-Graft-Polyaniline/Oxidized Dextran for Tissue Engineering. *Acta Biomater.* **2015**, *26*, 236−248.
(44) Al-Jallad, M.; Atassi, Y.; Mounif, E.; Aressy, M.; Tcharkhtchi, A. Oxidative Solution Polymerization of Aniline Hydrochloride Onto Electrospun Nanofibers Mats of Polylactic Acid: Preparation Method and Characterization. *J. Appl. Polym. Sci.* **2015**, *132*, 41618.
(45) Chen, J.; Yu, M.; Guo, B.; Ma, P. X.; Yin, Z. Conductive Nanofibrous Composite Scaffolds Based on In-Situ Formed Polyaniline Nanoparticle and Polylactide for Bone Regeneration. *J. Colloid Interface Sci.* **2018**, *514*, 517−527.
(46) Bers, D. M.; Despa, S. *Cardiac Excitation-Contraction Coupling. Encyclopedia of Biological Chemistry*: 2nd ed., 2013.
(47) Kléber, A. G.; Rudy, Y. Basic Mechanisms of Cardiac Impulse Propagation and Associated Arrhythmias. *Physiol. Rev.* **2004**, *84*, 431−488.
(48) DiFrancesco, D.; Tortora, P. Direct Activation of Cardiac Pacemaker Channels by Intracellular Cyclic AMP. *Nature* **1991**, *351*, 145−147.
(49) Mozaffarian, D.; Benjamin, E. J.; Go, A. S.; Arnett, D. K.; Blaha, M. J.; Cushman, M.; de Ferranti, S.; Després, J. P.; Fullerton, H. J.; Howard, V. J.; Huffman, M. D.; Judd, S. E.; Kissela, B. M.; Lackland, D. T.; Lichtman, J. H.; Lisabeth, L. D.; Liu, S.; Mackey, R. H.; Matchar, D. B.; McGuire, D. K.; Mohler, E. R., 3rd; Moy, C. S.; Muntner, P.; Mussolino, M. E.; Nasir, K.; Neumar, R. W.; Nichol, G.; Palaniappan, L.; Pandey, D. K.; Reeves, M. J.; Rodriguez, C. J.; Sorlie, P. D.; Stein, J.; Towfighi, A.; Turan, T. N.; Virani, S. S.; Willey, J. Z.; Woo, D.; Yeh, R. W.; Turner, M. B. Heart Disease and Stroke Statistics—2015 Update: A Report from the American Heart Association. *Circulation* **2014**, *131*, e29−e322.
(50) Bikkina, M.; Larson, M. G.; Levy, D. Asymptomatic ventricular arrhythmias and mortility risk in subjects withs with left ventricular hypertrophy. *J. Am. Coll. Cardiol.* **1993**, *22*, 1111−1116.
(51) Khan, R.; Sheppard, R. Fibrosis in heart disease: understanding the role of transforming growth factor-beta1 in cardiomyopathy, valvular disease and arrhythmia. *Immunology* **2006**, *118*, 10−24.
(52) Zhao, Y.; Feric, N. T.; Thavandiran, N.; Nunes, S. S.; Radisic, M. The Role of Tissue Engineering and Biomaterials in Cardiac Regenerative Medicine. *Can. J. Cardiol.* **2014**, *30*, 1307−1322.
(53) Stoppel, W. L.; Kaplan, D. L.; Black, L. D. Electrical and Mechanical Stimulation of Cardiac Cells and Tissue Constructs. *Adv. Drug Delivery Rev.* **2015**, *96*, 135−155.
(54) Radisic, M.; Park, H.; Shing, H.; Consi, T.; Schoen, F. J.; Langer, R.; Freed, L. E.; Vunjak-Novakovic, G. Functional Assembly of Engineered Myocardium by Electrical Stimulation of Cardiac Myocytes Cultured on Scaffolds. *Proc. Natl. Acad. Sci. U.S.A.* **2004**, *101*, 18129−18134.
(55) Chan, Y.-C.; Ting, S.; Lee, Y.-K.; Ng, K.-M.; Zhang, J.; Chen, Z.; Siu, C.-W.; Oh, S. K. W.; Tse, H.-F. Electrical Stimulation Promotes Maturation of Cardiomyocytes Derived from Human Embryonic Stem Cells. *J. Cardiovasc. Transl. Res.* **2013**, *6*, 989−999.
(56) Hernández, D.; Millard, R.; Sivakumaran, P.; Wong, R. C.; Crombie, D. E.; Hewitt, A. W.; Liang, H.; Hung, S. S.; Pébay, A.; Shepherd, R. K.; Dusting, G. J.; Lim, S. Y. Electrical Stimulation Promotes Cardiac Differentiation of Human Induced Pluripotent Stem Cells. *Stem Cells Int.* **2016**, *2016*, 1718041.
(57) Nunes, S. S.; Miklas, J. W.; Liu, J.; Aschar-Sobbi, R.; Xiao, Y.; Zhang, B.; Jiang, J.; Massé, S.; Gagliardi, M.; Hsieh, A.; Thavandiran, N.; Laflamme, M. A.; Nanthakumar, K.; Gross, G. J.; Backx, P. H.; Keller, G.; Radisic, M. Biowire: a platform for maturation of human pluripotent stem cell-derived cardiomyocytes. *Nat. Methods* **2013**, *10*, 781−787.
(58) Thavandiran, N.; Dubois, N.; Mikryukov, A.; Masse, S.; Beca, B.; Simmons, C. A.; Deshpande, V. S.; McGarry, J. P.; Chen, C. S.; Nanthakumar, K.; Keller, G. M.; Radisic, M.; Zandstra, P. W. Design

DOI: 10.1021/acsomega.8b03411
ACS Omega 2019, 4, 3660−3672

and Formulation of Functional Pluripotent Stem Cell-Derived Cardiac Microtissues. *Proc. Natl. Acad. Sci. U.S.A.* **2013**, *110*, E4698−E4707.
(59) You, J.-O.; Rafat, M.; Ye, G. J. C.; Auguste, D. T. Nanoengineering the Heart: Conductive Scaffolds Enhance Connexin 43 Expression. *Nano Lett.* **2011**, *11*, 3643−3648.
(60) Dvir, T.; Timko, B. P.; Brigham, M. D.; Naik, S. R.; Karajanagi, S. S.; Levy, O.; Jin, H.; Parker, K. K.; Langer, R.; Kohane, D. S. Nanowired Three-Dimensional Cardiac Patches. *Nat. Nanotechnol.* **2011**, *6*, 720−725.
(61) Wu, Y.; Wang, L.; Guo, B.; Ma, P. X. Interwoven Aligned Conductive Nanofiber Yarn/Hydrogel Composite Scaffolds for Engineered 3D Cardiac Anisotropy. *ACS Nano* **2017**, *11*, 5646−5659.
(62) Xu, C.; Huang, Y.; Yepez, G.; Wei, Z.; Liu, F.; Bugarin, A.; Tang, L.; Tong, Y. Development of Dopant-Free Conductive Bioelastomers. *Sci. Rep.* **2016**, *6*, 34451.
(63) Pivsa-Art, W.; Fujii, K.; Nomura, K.; Aso, Y.; Ohara, H.; Yamaone, H. The Effect of Poly(ethylene glycol) as Plasticizer in Blends of Poly(lactic acid) and Poly(butylene succinate). *J. Appl. Polym. Sci.* **2016**, *133*, 43044.
(64) Martin, O.; Avérous, L. Poly(lactic acid): Plasticization and Properties of Biodegradable Multiphase Systems. *Polymer* **2001**, *42*, 6209−6219.
(65) Hassouna, F.; Raquez, J.-M.; Addiego, F.; Dubois, P.; Toniazzo, V.; Ruch, D. New Approach on the Development of Plasticized Polylactide (PLA): Grafting of Poly(ethylene glycol) (PEG) Via Reactive Extrusion. *Eur. Polym. J.* **2011**, *47*, 2134−2144.
(66) Perez-Madrigal, M. M.; Llorens, E.; del Valle, L. J.; Puiggali, J.; Armelin, E.; Aleman, C. Semiconducting, Biodegradable and Bioactive Fibers for Drug Delivery. *eXPRESS Polym. Lett.* **2016**, *10*, 628−646.
(67) Reneker, D. H.; Yarin, A. L. Electrospinning Jets and Polymer Nanofibers. *Polymer* **2008**, *49*, 2387−2425.
(68) Baldissera, A. F.; de Miranda, K. L.; Bressy, C.; Martin, C.; Margaillan, A.; Ferreira, C. A. Using Conducting Polymers as Active Agents for Marine Antifouling Paints. *Mater. Res.* **2015**, *18*, 1129−1139.
(69) Atifi, S.; Hamad, W. Y. Emulsion-polymerized flexible semiconducting CNCs-PANI-DBSA nanocomposite films. *RSC Adv.* **2016**, *6*, 65494−65503.
(70) Kister, G.; Cassanas, G.; Vert, M. Effects of morphology, conformation and configuration on the IR and Raman spectra of various poly(lactic acid)s. *Polymer* **1998**, *39*, 267−273.
(71) Nobrega, M. M.; Silva, C. H. B.; Constantino, V. R. L.; Temperini, M. L. A. Spectroscopic Study on the Structural Differences of Thermally Induced Cross-Linking Segments in Emeraldine Salt and Base Forms of Polyaniline. *J. Phys. Chem. B* **2012**, *116*, 14191−14200.
(72) Shakoor, A.; Rizvi, T. Z. Raman spectroscopy of conducting poly (methyl methacrylate)/polyaniline dodecylbenzenesulfonate blends. *J. Raman Spectrosc.* **2010**, *41*, 237−240.
(73) Salvatierra, R. V.; Moura, L. G.; Oliveira, M. M.; Pimenta, M. A.; Zarbin, A. J. G. Resonant Raman Spectroscopy and Spectroelectrochemistry Characterization of Carbon Nanotubes/Polyaniline Thin Film Obtained Through Interfacial Polymerization. *J. Raman Spectrosc.* **2012**, *43*, 1094−1100.
(74) del Valle, L. J.; Camps, R.; Díaz, A.; Franco, L.; Rodríguez-Galán, A.; Puiggalí, J. Electrospinning of Polylactide and Polycaprolactone Mixtures for Preparation of Materials with Tunable Drug Release Properties. *J. Polym. Res.* **2011**, *18*, 1903−1917.
(75) Kim, J.; Kwon, S.; Ihm, D. Synthesis and Characterization of Organic Soluble Polyaniline Prepared by One-Step Emulsion Polymerization. *Curr. Appl. Phys.* **2007**, *7*, 205−210.

DOI: 10.1021/acsomega.8b03411
ACS Omega 2019, 4, 3660−3672